Scientific Research Publishing

Open Journal of Applied Sciences, 2026, 16(6), 2012-2020
https://www.scirp.org/journal/ojapps
ISSN Online: 2165-3925
ISSN Print: 2165-3917

Bloch Surface Waves with TM Polarization in the Ternary Multilayer

Bingmei Wei, Yufu Jiang, Junxue Chen

College of Physics and Electronic Information Engineering, Guilin University of Technology, Guilin, China
Email: 2195125399@qq.com

How to cite this paper: Wei, B.M., Jiang, Y.F. and Chen, J.X. (2026) Bloch Surface Waves with TM Polarization in the Ternary Multilayer. *Open Journal of Applied Sciences*, **16**, 2012-2020.
https://doi.org/10.4236/ojapps.2026.166111

Received: May 28, 2026
Accepted: June 1, 2026
Published: June 4, 2026

Abstract

In the one-dimensional binary dielectric multilayer, the structure cannot support TM polarized Bloch surface waves (TM-BSW) near the Brewster angle due to the existence of the Brewster effect, which limits the related applications of BSW. In this work, the photonic bandgap and the dispersion behaviors of Bloch surface waves in a ternary dielectric structure were investigated. The Brewster effect of the structure is broken by introducing an additional dielectric layer into the binary structure. The zero photonic bandgap caused by the Brewster angle effect in the multilayer substrate is eliminating. This enables effective control of TM-BSW like TE-BSW in the truncated ternary structure. The research results enrich the study of Bloch surface waves and have potential applications in polarization related surface wave devices.

Keywords

Bloch Surface Waves, TM Polarization, Brewster Effect, Photonic Bandgap

1. Introduction

Surface electromagnetic waves (SEW) propagate along the interface between two media with different properties and can be strongly confined with huge field enhancement at the surface. One of the best-known examples of SEW is surface plasmon polaritons (SPPs), which are guided along the interfaces between dielectrics and metals. The SPP has been attracted great attention in the last decade due to the wide applications in surface enhanced Raman scattering (SERS) [1] [2], enhanced nonlinear optical effects [3] [4], highly sensitive biological and chemical sensors [5] [6]. Alternatively, Bloch surface waves (BSW) can be formed at the surface of a one-dimensional photonic crystal (1DPC). The BSW exploited the band gap of the 1DPC to obtain the guiding of a surface wave thus giving rise to a

surface sensitive evanescent field [7] [8]. Due to the use of dielectric materials with low loss, the BSW have much longer propagation distance compared to that of SPPs. As a promising alternative to the plasmonic device, BSW has become one of researching hotspots in photonics with a wide range of applications ranging from fluorescence enhancement, label-free sensing, to nano waveguide and more [9]-[13].

Although the 1DPC can sustain the propagation of BSW with TE and TM polarization, many attentions are currently concentrated on the TE BSW. One of the reasons is the difference of band gap between TE and TM polarization in the 1DPC. In the one-dimensional binary PC consisted by alternating the dielectric layers with high and low refraction index, the band gap with TM polarization will be disappeared at the Brewster angle due to the decoupling between the incident and reflected waves. Then, the TM BSW cannot be formed in this region for the one-dimensional binary PC, which prevents the applications of TM BSW as that of TE BSW. However, TM polarized surface waves have richer intrinsic properties, such as spin momentum locking effect [14] [15], which can be used to mimic the quantum spin Hall effect and generate new applications.

The one-dimensional ternary periodic structure can be formed by sandwiching the third material between the two materials with different properties. Then, there are three material layers constituting a period of lattice in the one-dimensional ternary PC. Due to the increased interface reflection as the waves propagation through a period of lattice, the one-dimensional ternary PC structures demonstrated some different electromagnetic behaviors compared to that of the one-dimensional binary PC. The ternary periodic structures were used to enlarge the bandgap frequency range of the omnidirectional total reflection [16]-[18] and extend the zero-effective-phase photonic bandgap [19]. However, there aren't any papers discussing the properties of BSW sustained by a truncated one-dimensional ternary PC structure, although the BSW are widely studied in the binary periodic structure. In this work, the BSW with TM polarization sustained by a truncated one-dimensional ternary PC structure are theoretically studied. Different from the BSW in the binary PC, the dispersion of TM BSW is not broken off at the Brewster angle, and can be engineered in wide frequency range as that of the TE BSW in the ternary PC by adjusting the material compositions and geometrical size of the lattice. Therefore, the TM BSW in the ternary PC can be used to mimic the similar electromagnetic phenomena related to the SPPs due to the same polarization state.

2. Band Structures in Ternary Multilayer

The considered ternary dielectric structure is shown in **Figure 1**. The truncated one-dimensional periodic ternary structure consists of thin films of three dielectric materials, with refractive indices of n_1, n_2, and n_3 and thicknesses of d_1, d_2, and d_3, respectively. The unit period $\Lambda = d_1 + d_2 + d_3$. At the top of the structure, there is a dielectric layer with a refractive index of n_2 and a thickness of d_a to sup-

port the propagation of BSW. General features of the photonic band structure of the semi-infinite periodic structure can be understood through the properties of the infinite periodic structure. In the infinite periodic structure, the dielectric function $\varepsilon(r)$ varies periodically with z and is invariant in the y and x directions. Then, for the TM polarization (the magnetic field is perpendicular to the x-z plane), the magnetic field is given in the Bloch-wave form.

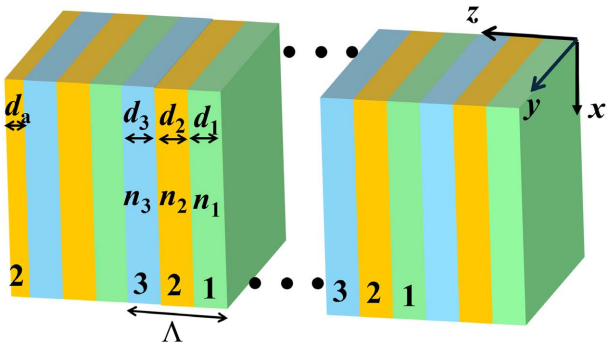

Figure 1. Schematic diagram of truncated one-dimensional periodic ternary dielectric structure. The unit cell of the structure consists of three different dielectric layers (refraction index n_j, film thickness d_j). An additional layer with refraction index n_2 and thickness d_a is introduced on top of the structure to support the propagation of BSW.

$$H_{y,K}(x,z) = H_{y,K}(z)\mathrm{e}^{jKz}\mathrm{e}^{j\beta x} \tag{1}$$

where K is the Bloch wave number, β is the wave vector parallel to the interface, $H_{y,K}(z)$ is periodic function with a period Λ. The magnetic field in each layer of the nth cell can be written as the combination of two plane waves propagating along the opposite directions [2].

$$H_{y,K}^{(n,j)} = \left[a_j\mathrm{e}^{i\gamma_j(z-n\Lambda)} + b_j\mathrm{e}^{-i\gamma_j(z-n\Lambda)}\right]\mathrm{e}^{i\beta x}\mathrm{e}^{iKn\Lambda} \tag{2}$$

where $\gamma_j = \sqrt{k_0^2 n_j^2 - \beta^2}$ is the wave vector along the z direction.

$$j = \begin{cases} 1, & n\Lambda < z < n\Lambda + d_1 \\ 2, & n\Lambda + d_1 < z < n\Lambda + d_1 + d_2 \\ 3, & n\Lambda + d_1 + d_2 < z < (n+1)\Lambda \end{cases} \tag{3}$$

Applying the continuity boundary condition at $z = n\Lambda + d_1$, $z = n\Lambda + d_1 + d_2$ and $z = (n+1)\Lambda$, the Bloch wave satisfies the following eigenvalue equation.

$$\begin{pmatrix} A & B \\ C & D \end{pmatrix}\begin{pmatrix} a_j \\ b_j \end{pmatrix} = \mathrm{e}^{iK\Lambda}\begin{pmatrix} a_j \\ b_j \end{pmatrix} \tag{4}$$

where the matrix element A, B, C and D are obtained as:

$$\begin{aligned} A = \frac{\mathrm{e}^{i\gamma_1 d_1}}{2}\Big\{&\cos\gamma_2 d_2\left[2\cos\gamma_3 d_3 + i(g_{31}+g_{13})\sin\gamma_3 d_3\right] \\ &+ i\sin\gamma_2 d_2\left[(g_{12}+g_{21})\cos\gamma_3 d_3 + i(g_{23}+g_{32})\sin\gamma_3 d_3\right]\Big\} \end{aligned} \tag{5}$$

$$B = \frac{je^{-j\gamma_1 d_1}}{2}\left\{\left(g_{31}-g_{13}\right)\cos\gamma_2 d_2 \sin\gamma_3 d_3 + \sin\gamma_2 d_2\left[\left(g_{21}-g_{12}\right)\cos\gamma_3 d_3 + i\left(g_{23}-g_{32}\right)\sin\gamma_3 d_3\right]\right\} \tag{6}$$

$$C = \frac{-je^{j\gamma_1 d_1}}{2}\left\{\left(g_{31}-g_{13}\right)\cos\gamma_2 d_2 \sin\gamma_3 d_3 + \sin\gamma_2 d_2\left[\left(g_{21}-g_{12}\right)\cos\gamma_3 d_3 - i\left(g_{23}-g_{32}\right)\sin\gamma_3 d_3\right]\right\} \tag{7}$$

$$D = \frac{e^{-i\gamma_1 d_1}}{2}\left\{\cos\gamma_2 d_2\left[2\cos\gamma_3 d_3 - i\left(g_{31}+g_{13}\right)\sin\gamma_3 d_3\right] - i\sin\gamma_2 d_2\left[\left(g_{12}+g_{21}\right)\cos\gamma_3 d_3 - i\left(g_{23}+g_{32}\right)\sin\gamma_3 d_3\right]\right\} \tag{8}$$

where $g_{ij} = 1/g_{ji}\ (i,j=1,2,3)$. For TM polarization $g_{ij} = \left(\gamma_i n_j^2\right)/\left(\gamma_j n_i^2\right)$, For TE polarization $g_{ij} = \gamma_i/\gamma_j$. According to the eigenvalue Equation (4), the dispersion relation for the propagation of the electromagnetic wave in the infinite periodic structure can be obtained as

$$\begin{aligned}\cos K\Lambda &= \frac{A+D}{2}\\ &= \cos\gamma_1 d_1 \cos\gamma_2 d_2 \cos\gamma_3 d_3\\ &\quad -\frac{1}{2}\left(g_{31}+g_{13}\right)\sin\gamma_1 d_1 \cos\gamma_2 d_2 \sin\gamma_3 d_3\\ &\quad -\frac{1}{2}\left(g_{12}+g_{21}\right)\sin\gamma_1 d_1 \sin\gamma_2 d_2 \cos\gamma_3 d_3\\ &\quad -\frac{1}{2}\left(g_{23}+g_{32}\right)\cos\gamma_1 d_1 \sin\gamma_2 d_2 \sin\gamma_3 d_3\end{aligned} \tag{9}$$

The Bloch wave number K can be real or imaginary values, corresponding to the propagating or evanescent Bloch wave, respectively. Then, the solution of Equation (9) defines the photonic band structure for the infinite periodic structure, $\omega(K,\beta)$. Regimes where $\left|\cos(K\Lambda)\right| > 1$, K has an imaginary part, and the Bloch wave is evanescent. It corresponds to the stop bands for the periodic medium. When $\left|\cos(K\Lambda)\right| < 1$ correspond to the real K and the Bloch wave is propagating.

In simulation, the dielectrics are lossless, isotropic, and dispersion-free over the analyzed frequency range. The unit period Λ is fixed at 230 nm for the binary and ternary periodic structure for the convenience of comparing photon energy bands.

Figure 2(a) shows the projected photonic band structure for a binary periodic structure. The cyan regions denote the phase space where the K is imaginary, that is, regions of the evanescent states, whereas carmine areas represent the regions of propagating states. It is noted that the stop band shrink to zero as $\beta = k_0 n_1 \sin\theta_B$ with $\theta_B = \arctan\left(n_3/n_1\right)$ as the Brewster angle, since at this angle the incident wave is not reflected at the interface of film. Then, the TM BSW cannot be supported at this angle.

In Figure 2(b) we show the projected photonic band structure for a ternary periodic structure. In the unit cell, there are three dielectric layers with two interfaces. As the electromagnetic wave is incident at the Brewster angle of adjacent dielectric layer, the wave will be reflected at the other interface. Then, the incident

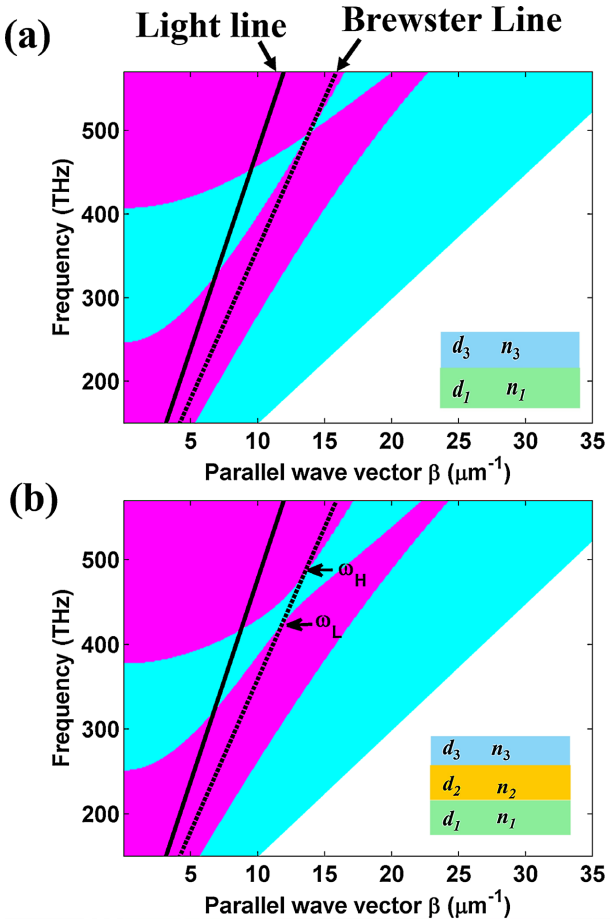

Figure 2. (a) Projected photonic band structure of a binary periodic structure with the light line and Brewster line. The film parameters are $n_1 = 1.46$, $n_3 = 3.22$, $d_1 = 160$ nm and $d_2 = 70$ nm. (b) Projected photonic band structure of a ternary periodic structure together with the light line and Brewster line. The film parameters are $n_1 = 1.46$, $n_2 = 2.3$, $n_3 = 3.22$, and the thickness $d_1 = 120$ nm, $d_2 = 60$ nm, $d_3 = 50$ nm. The cyan regions denote the photonic stop band of the structure in which light cannot propagate through the multilayer. The unit cell is shown in the inset.

and reflected waves will be coupled, and formed the bandgap. The extent of bandgap is well related to the contrast of the refraction indices in the unit cell. For example, as the wave is incident at the Brewster angle, the exact expression for the band edges is obtained as:

$$\begin{aligned}&\cos\gamma_1 d_1 \cos\gamma_2 d_2 \cos\gamma_3 d_3 - \sin\gamma_1 d_1 \cos\gamma_2 d_2 \sin\gamma_3 d_3 \\ &-\frac{1}{2}\left(\alpha+\frac{1}{\alpha}\right)\sin\gamma_1 d_1 \sin\gamma_2 d_2 \cos\gamma_3 d_3 \\ &-\frac{1}{2}\left(\alpha+\frac{1}{\alpha}\right)\cos\gamma_1 d_1 \sin\gamma_2 d_2 \sin\gamma_3 d_3 + 1 = 0\end{aligned} \tag{10}$$

where $\alpha = n_2^2 \Big/ \sqrt{n_2^2\left(n_1^2+n_3^2\right)-n_1^2 n_3^2}$. As the thickness $d_2 \to 0$ (*i.e.* binary multilayer structure), the upper and lower band edges will be intersected, and the corresponding frequency in the intersection point in the first harmonic is $f = c\sqrt{n_1^2+n_3^2} \Big/ \left[2n_1^2\left(\Lambda - d_3\right)+2n_3^2 d_3\right]$. For the finite thickness d_2, the upper and

lower band edge will be separated due to the Bragg reflection. The separated frequency is determined by solving the Equation (10). A dimensionless parameter η is used to quantify the extent of separation between upper and lower band edges, and is defined as $\eta = 2(\omega_H - \omega_L)/(\omega_H + \omega_L)$, where ω_H and ω_L are determined by solving the Equation (10).

Figure 3 shows the ratio η as a function of the n_2/n_1 and n_3/n_2. The contours in this figure represent various bandgap ranges for different refractive index parameters. It is noted that the photonic bandgap width increases with the increase of refractive index contrast. The refractive index contrast and bandgap width of the ternary materials used in this work are represented by dashed lines and symbol circles in the figure, respectively. It is noted that the frequency separation η can reach 15.8%. Then, a bandgap at the Brewster angle can be observed in the ternary periodic structure as shown in Figure 2(b).

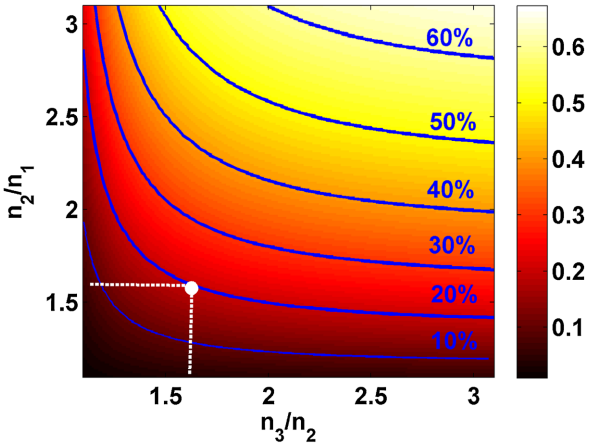

Figure 3. The range to midrange ratio η as a function of the n_2/n_1 and n_3/n_2. The results were obtained at the Brewster angle in the first photonic bandgap. Here, the thicknesses of the layers were set as one sixth wavelength.

3. Dispersion Behaviors of BSW in the Ternary PC

In Figure 1, the semi-infinite periodic structure is created by replacing the part of the infinite periodic structure lying in the region $-\infty < z < 0$ by dielectric layer with refractive indices n_2 and film thickness d_a. The BSW are solutions of Maxwell's equations in which the waves are localized at surface of the semi-infinite periodic structure, and the field amplitude is evanescent in both periodic structure and environmental dielectric with refractive index ne. According to the continuity boundary conditions, the dispersion equation of TM-BSW in truncated ternary multilayers can be obtained as

$$Z_B + Z_G = 0 \tag{11}$$

$$Z_B = \frac{\dfrac{\gamma_e}{\varepsilon_e} - i\dfrac{\gamma_2}{\varepsilon_2}\tan(\gamma_2 d_a)}{\dfrac{\gamma_2}{\varepsilon_2}\dfrac{\dfrac{\gamma_2}{\varepsilon_2} - i\dfrac{\gamma_e}{\varepsilon_e}\tan(\gamma_2 d_a)}{}} \tag{12}$$

$$Z_G = \frac{\gamma_3}{\varepsilon_3}\frac{B - e^{jK\Lambda} + A}{B + e^{jK\Lambda} - A} \tag{13}$$

where Z_B is the equivalent impedance of dielectric layer on the top of structure, Z_G is the equivalent impedance of the truncated ternary multilayers. In Equation (13), the coefficients A and B are given in Equations (5) and (6).

Figure 4(a) shows the dispersion relation of TM-polarized BSW by solving the Equation (11). The dispersion curve of TM BSW is sited in the bandgap region and below the light line. It contributes to the evanescent behavior of field in the multilayer and the environmental medium. Moreover, similar to the TE BSW, the dispersion of TM BSW can be engineered in wide frequency range without the influence of the Brewster effect. The TM BSW can be sustained by the truncated ternary multilayers above 385 THz as shown in Figure 4(a). The electric field amplitude distribution of TM BSW at wavelength of 760 nm is shown in Figure 4(b). As expected, the electric field is strongly peaked at the interface between the multilayer and air. The attenuation of wave in the multilayer depends on the refractive index contrast in the unit cell. Whereas the exponential decay in the

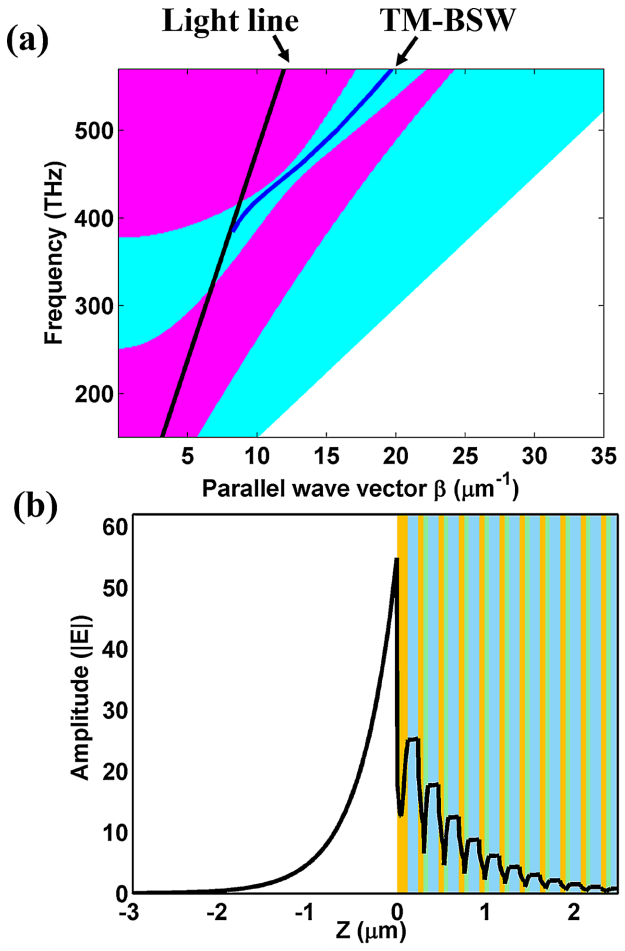

Figure 4. (a) Projected band structure and BSW dispersion relation (solid blue) for a semi-infinite ternary multilayer with d_a = 120 nm for TM polarization. (b) Electric field amplitude distribution in the ternary multilayer for the TM BSW at wavelength of 400 THz.

environmental medium is only determined by the refraction index ne as the parallel wave vector β is fixed. Thus, the TM-BSW exhibits evanescent behaviors in both the environmental medium and the dielectric multilayers, which has the intrinsic spin-momentum locking effect as that of surface plasmon polaritons (SPPs) [20].

4. Conclusion

In summary, we have theoretically studied the dispersion behaviors of BSW in a truncated one-dimensional periodic ternary multilayer. Different from the binary structure, the Brewster effect is inhibited in the ternary structure due to the additional interface reflection of waves. The photonic bandgap can also be formed around the Brewster angle. The bandgap width can be engineered by changing the refractive index contrast in the ternary multilayer. The BSW with TM polarization can be sustained in wide frequency range as that of TE-BSW in the truncated ternary multilayer. Our work has potential applications in various areas, such as polarization transformation devices, biosensing, and imaging, among others.

Conflicts of Interest

The authors declare no conflicts of interest regarding the publication of this paper.

References

[1] Li, N., Wang, X., Tibbs, J., Che, C., Peinetti, A.S., Zhao, B., *et al.* (2021) Label-Free Digital Detection of Intact Virions by Enhanced Scattering Microscopy. *Journal of the American Chemical Society*, **144**, 1498-1502. https://doi.org/10.1021/jacs.1c09579

[2] Kneipp, K., Wang, Y., Kneipp, H., Perelman, L.T., Itzkan, I., Dasari, R.R., *et al.* (1997) Single Molecule Detection Using Surface-Enhanced Raman Scattering (SERS). *Physical Review Letters*, **78**, 1667-1670. https://doi.org/10.1103/physrevlett.78.1667

[3] Khurgin, J.B. and Sun, G. (2013) Plasmonic Enhancement of the Third Order Nonlinear Optical Phenomena: Figures of Merit. *Optics Express*, **21**, Article 27460. https://doi.org/10.1364/oe.21.027460

[4] Verhagen, E., Kuipers, L. and Polman, A. (2007) Enhanced Nonlinear Optical Effects with a Tapered Plasmonic Waveguide. *Nano Letters*, **7**, 334-337. https://doi.org/10.1021/nl062440f

[5] Hojjat Jodaylami, M., Masson, J. and Badia, A. (2025) Surface Plasmon Resonance Sensing. *Nature Reviews Methods Primers*, **5**, Article No. 47. https://doi.org/10.1038/s43586-025-00417-8

[6] Biswas, A., Lee, S., Cencillo-Abad, P., Karmakar, M., Patel, J., Soudi, M., *et al.* (2024) Nanoplasmonic Aptasensor for Sensitive, Selective, and Real-Time Detection of Dopamine from Unprocessed Whole Blood. *Science Advances*, **10**, eadp7460. https://doi.org/10.1126/sciadv.adp7460

[7] Meade, R.D., Brommer, K.D., Rappe, A.M. and Joannopoulos, J.D. (1991) Electromagnetic Bloch Waves at the Surface of a Photonic Crystal. *Physical Review B*, **44**, 10961-10964. https://doi.org/10.1103/physrevb.44.10961

[8] Yeh, P., Yariv, A. and Hong, C. (1977) Electromagnetic Propagation in Periodic Strat-

ified Media I General Theory. *Journal of the Optical Society of America*, **67**, 423-438. https://doi.org/10.1364/josa.67.000423

[9] Descrovi, E., Sfez, T., Quaglio, M., Brunazzo, D., Dominici, L., Michelotti, F., *et al.* (2010) Guided Bloch Surface Waves on Ultrathin Polymeric Ridges. *Nano Letters*, **10**, 2087-2091. https://doi.org/10.1021/nl100481q

[10] Sinibaldi, A., Fieramosca, A., Rizzo, R., Anopchenko, A., Danz, N., Munzert, P., *et al.* (2014) Combining Label-Free and Fluorescence Operation of Bloch Surface Wave Optical Sensors. *Optics Letters*, **39**, 2947-2950. https://doi.org/10.1364/ol.39.002947

[11] Soboleva, I.V., Moskalenko, V.V. and Fedyanin, A.A. (2012) Giant Goos-Hänchen Effect and Fano Resonance at Photonic Crystal Surfaces. *Physical Review Letters*, **108**, Article 123901. https://doi.org/10.1103/physrevlett.108.123901

[12] Yu, L., Barakat, E., Sfez, T., Hvozdara, L., Di Francesco, J. and Peter Herzig, H. (2014) Manipulating Bloch Surface Waves in 2D: A Platform Concept-Based Flat Lens. *Light: Science & Applications*, **3**, e124. https://doi.org/10.1038/lsa.2014.5

[13] Badugu, R., Mao, J., Blair, S., Zhang, D., Descrovi, E., Angelini, A., *et al.* (2016) Bloch Surface Wave-Coupled Emission at Ultraviolet Wavelengths. *The Journal of Physical Chemistry C*, **120**, 28727-28734. https://doi.org/10.1021/acs.jpcc.6b08086

[14] Shi, P., Du, L. and Yuan, X. (2021) Spin Photonics: From Transverse Spin to Photonic Skyrmions. *Nanophotonics*, **10**, 3927-3943. https://doi.org/10.1515/nanoph-2021-0046

[15] Picardi, M.F., Zayats, A.V. and Rodríguez-Fortuño, F.J. (2018) Janus and Huygens Dipoles: Near-Field Directionality beyond Spin-Momentum Locking. *Physical Review Letters*, **120**, Article 117402. https://doi.org/10.1103/physrevlett.120.117402

[16] Awasthi, S.K., Malaviya, U. and Ojha, S.P. (2006) Enhancement of Omnidirectional Total-Reflection Wavelength Range by Using One-Dimensional Ternary Photonic Bandgap Material. *Journal of the Optical Society of America B*, **23**, 2566-2571. https://doi.org/10.1364/josab.23.002566

[17] Wang, S., Yang, X. and Liu, C.T. (2014) Omnidirectional Reflection in One-Dimensional Ternary Photonic Crystals and Photonic Heterostructures. *Physics Letters A*, **378**, 1326-1332. https://doi.org/10.1016/j.physleta.2014.03.010

[18] Gharaati, A. and Zare, Z. (2011) Photonic Band Structures and Enhancement of Omnidirectional Reflection Bands by Using a Ternary 1D Photonic Crystal Including Left-Handed Materials. *Progress in Electromagnetics Research M*, **20**, 81-94.

[19] Xiang, Y., Dai, X., Wen, S., Tang, Z. and Fan, D. (2011) Extending the Zero-Effective-Phase Photonic Bandgap by One-Dimensional Ternary Photonic Crystals. *Applied Physics B*, **103**, 897-906. https://doi.org/10.1007/s00340-011-4439-x

[20] Van Mechelen, T. and Jacob, Z. (2016) Universal Spin-Momentum Locking of Evanescent Waves. *Optica*, **3**, 118-126. https://doi.org/10.1364/optica.3.000118